Ionic contribution to the self-potential signals associated with a redox front

A. Revil, F. Trolard, J. Castermant, Abderrahim Jardani, C.A. Mendonça

Journal of Contaminant Hydrology 109 (2009) 27–39

Contents lists available at ScienceDirect

Journal of Contaminant Hydrology

journal homepage: www.elsevier.com/locate/jconhyd

Ionic contribution to the self-potential signals associated with a redox front

A. Revil [a,b,*], F. Trolard [c], G. Bourrié [c], J. Castermant [c], A. Jardani [a,1], C.A. Mendonça [d]

[a] Colorado School of Mines, Dept. of Geophysics, Golden, CO, USA
[b] CNRS-LGIT (UMR 5559), University of Savoie, Equipe Volcan, Le Bourget-du-Lac, France
[c] INRA, UR 1119, Géochimies des Sol et des Eaux, F13545 Aix en Provence, France
[d] Instituto de Astronomia, Geofísica e Ciências Atmosféricas, São Paulo, Brazil

ARTICLE INFO

Article history:
Received 8 November 2008
Received in revised form 29 July 2009
Accepted 30 July 2009
Available online 11 August 2009

Keywords:
Self-potential
Redox potential
Contaminant plume
pH
Sandbox

ABSTRACT

In contaminant plumes or in the case of ore bodies, a source current density is produced at depth in response to the presence of a gradient of the redox potential. Two charge carriers can exist in such a medium: electrons and ions. Two contributions to the source current density are associated with these charge carriers (i) the gradient of the chemical potential of the ionic species and (ii) the gradient of the chemical potential of the electrons (i.e., the gradient of the redox potential). We ran a set of experiments in which a geobattery is generated using electrolysis reactions of a pore water solution containing iron. A DC power supply is used to impose a difference of electrical potential of 3 V between a working platinum electrode (anode) and an auxiliary platinum electrode (cathode). Both electrodes inserted into a tank filled with a well-calibrated sand infiltrated by a (0.01 mol L^{-1} KCl + 0.0035 mol L^{-1} $FeSO_4$) solution. After the direct current is turned off, we follow the pH, the redox potential, and the self-potential at several time intervals. The self-potential anomalies amount to a few tens of millivolts after the current is turned off and decreases over time. After several days, all the redox-active compounds produced initially by the electrolysis reactions are consumed through chemical reactions and the self-potential anomalies fall to zero. The resulting self-potential anomalies are shown to be much weaker than the self-potential anomalies observed in the presence of an electronic conductor in the laboratory or in the field. In the presence of a biotic or an abiotic electronic conductor, the self-potential anomalies can amount to a few hundred millivolts. These observations point out indirectly the potential role of bacteria forming biofilms in the transfer of electrons through sharp redox potential gradient in contaminant plumes that are rich in organic matter.

1. Introduction

Characterization of redox zones is an important goal for the evaluation of the natural attenuation and remediation processes of contaminated areas in downstream landfills (Tuccillo et al., 1999; Christensen et al., 2000; Personna et al., 2008). However, in situ measurements of the redox potential in contaminant plumes are a difficult task (Christensen et al., 2000). The existence of a non-intrusive redox sensor would be therefore an important tool to characterize and image the redox processes occurring in contaminant plumes and to determine non-intrusively the activity of redox-active species. Does such a non-intrusive geophysical method can be developed? We know that contaminant plumes that are rich in organic matter are the setting of electrical currents (Naudet et al., 2003, 2004; Naudet and Revil, 2005; Arora et al., 2007; Linde and Revil, 2007). The occurrence of such a geobattery can be evidenced through the passive measurement of the electrical potential distribution at the ground surface of the Earth, a method known in geophysics as the self-potential method.

The self-potential method is one of the oldest geophysical method (Fox, 1830; Bolève et al., 2007; Crespy et al., 2007). It consists in mapping or monitoring the electrical potential distribution occurring at the surface of the Earth (or possibly

* Corresponding author. Colorado School of Mines, Green Center, Dept of Geophysics, Golden, CO, 80401, USA. Tel.: +1 303 273 3512.
E-mail address: arevil@mines.edu (A. Revil).
[1] Now at M2C, UMR 6143, CNRS, Morphodynamique Continentale et Côtière, Université de Rouen, 76821 Mont Saint Aignan, France.

0169-7722/$ – see front matter © 2009 Elsevier B.V. All rights reserved.
doi:10.1016/j.jconhyd.2009.07.008

in boreholes) using a set of non-polarizing or capacitive electrodes and a high-input impedance (>10 MΩ) voltmeter with generally a sensitivity of at least 0.1 mV. In self-potential mapping, an electrode (called the reference electrode) is used as a fixed reference in the field at a base station (generally upstream) (Naudet et al., 2003, 2004; Arora et al., 2007). A second electrode (called the roving electrode) is used to scan the value of the electrical potential at various stations with respect to the electrical potential of the base station. Anomalous signals with respect to the base station are called self-potential anomalies (Corwin and Hoover, 1979).

The existence of a geobattery generating self-potential anomalies is well known in mineral exploration (e.g., Sivenas and Beales, 1982; Stoll et al., 1995; Bigalke and Grabner, 1997; Mendonça, 2008). The concept of geobattery was established by Sato and Mooney (1960) and a non-linear mechanistic model was developed later by Stoll et al. (1995) and Bigalke and Grabner (1997) based on the Butler–Volmer equation developed in electrochemistry (Bockris and Reddy, 1970; Peiffer et al., 1992). The Butler–Volmer equation has been used to account for the activation energy between electron donors and the ore body (acting as a passive electrode) and between the ore body and electron acceptors (O_2 is generally the terminal electron acceptor). Such a geobattery model connects non-linearly the source current density to the distribution of the activity of electron donors and electron acceptors in the vicinity of the ore body.

For contaminant plumes that are rich in organic matter, very strong (>300 mV) self-potential anomalies have been observed in the field (Naudet et al., 2003, 2004; Arora et al., 2007; Linde and Revil, 2007). To explain these anomalies, a geobattery model was suggested by Naudet et al. (2003, 2004) and later modeled by Arora et al. (2007) and Linde and Revil (2007) using a phenomenological relationship between the source current density and the redox potential. This relationship was first developed empirically using field observation (Naudet et al., 2003, 2004). A plausible mechanism for the transfer of electrons between the reduced and oxidized portions of the ground was proposed recently by Ntarlagiannis et al. (2007). This proposed mechanism was based on the formation of conductive pili (called nanowires) between bacteria in a biofilm that may be able to transmit electrons through a sharp redox front from electron donors to electron acceptors. Such electron transfer may involve the symbioses of different bacterial communities.

In this paper, we consider the case of a sharp redox potential distribution generated in a water-saturated porous medium with no electron conductor present to bridge electron donors and acceptors in the system. These experiments demonstrate that despite the absence of electron conductors, self-potential anomalies can be observed. However, their magnitudes are much weaker than in the case of the geobattery associated with an abiotic electronic conductor (Castermant et al., 2008) or with a biotic electronic conductor associated with the conductive pili of some bacteria (Ntarlagiannis et al., 2007).

2. Background

The existence of electrical potential anomalies is associated with natural source currents occurring in the ground (e.g., Maineult et al., 2004, 2005, 2006; Crespy et al., 2008). Various sources of self-potential signals exist in nature. For example the streaming current is a source current density associated with the flow of pore water and the thermoelectric current is a source of current associated with the influence of temperature upon the chemical potential of ionic species or electrons (Revil, 1999). A unified model incorporating these effects for the source current density $\mathbf{j}_S$ (in A m^{-2}) has been proposed recently by Revil and Linde (2006). A general model of self-potential signals in porous materials is given by solving the following two equations for the total current density $\mathbf{j}$,

$$\nabla \cdot \mathbf{j} = 0, \tag{1}$$

$$\mathbf{j} = \sigma \mathbf{E} + \mathbf{j}_S. \tag{2}$$

where $\mathbf{E}$ is the electrical field (in V m^{-1}). Eq. (1) is the quasi-static continuity equation for the charge. It implies that the flux of charges is conservative (no storage of charges). Eq. (2) is a generalized Ohm's law with a source current density $\mathbf{j}_S$. In the quasi-static limit of the Maxwell equations, the electrical field $\mathbf{E} = -\nabla\psi$ can be derived directly from an electrostatic potential ψ (in V) to ensure that $\nabla \times \mathbf{E} = 0$.

According to the model developed by Revil and Linde (2006, equation 182), the source current density associated with gradients of the activity (or chemical potential) of the charge carriers is,

$$\mathbf{j}_S = -k_b T \sum_{i=1}^{N+1} \frac{t_i \sigma}{q_i} \nabla ln\{i\}, \tag{3}$$

where the sum is extended to N-ionic species plus the electrons acting as an additional charge carrier, k_b is the Boltzmann constant (in J K^{-1}), T is the absolute temperature (in K), q_i is the charge of species i (in C), t_i is the microscopic Hittorf number of the ionic species i in the pore water, σ is the total electrical conductivity of the porous material, and $\{i\}$ represents the activity of the species i. The microscopic Hittorf number of the electrons represents the fraction of the total current transported by the electrons and can be defined from a model of electronic conduction inside the pore space of the porous material like the conductive pili of bacteria as discussed further in Section 5 below. No free electrons exist in water.

Eq. (3) implies that two contributions may exist to compute self-potential signals associated with concentrations of the charge carriers. The first contribution is related to the gradient of the chemical potential of all the ionic species that are present in the pore water. This contribution is called the diffusion current (Cussler, 2008). This process is at the origin of the well-known diffusion potential in electrochemistry (Maineult et al., 2006; Revil and Linde, 2006 and reference therein) and the self-potential signals in boreholes in sedimentary basins (Doll, 1949). The second contribution is related to the activity of the electrons and is called the electro-redox current density (see recent abiotic experiments by Castermant et al., 2008 and biotic experiments by Ntarlagiannis et al., 2007). Because electrons do not freely exist in water, this contribution requires a biotic or an abiotic electronic conductor. This contribution will be discussed in more details in Section 5.

In the next sections, we are interested by the self-potential signals associated with the gradient of the chemical potential of the ionic species in the pore water and especially by their magnitude.

3. Experimental setup

The equipment we used consists of a generator of direct current, a working platinum (Pt) electrode (labeled WE below and corresponding to the anode, Radiometer analytical®, XM-140 type), an auxiliary platinum electrode (labeled AE below and corresponding to the cathode, Radiometer analytical®, XM-140 type), one or two Plexiglas™ sandboxes, an electrolyte of known composition (Fig. 1a), a potentiostat/galvanostat generator (Tacussel®, PTJ 16-0.6 type), one reference electrode Ag/AgCl (denoted "Ref") (Radiometer analytical®, REF321/XR300 type.

Two experiments were performed and in both, the water table was maintained constant. In the first experiment, the WE and AE electrodes were located inside the same

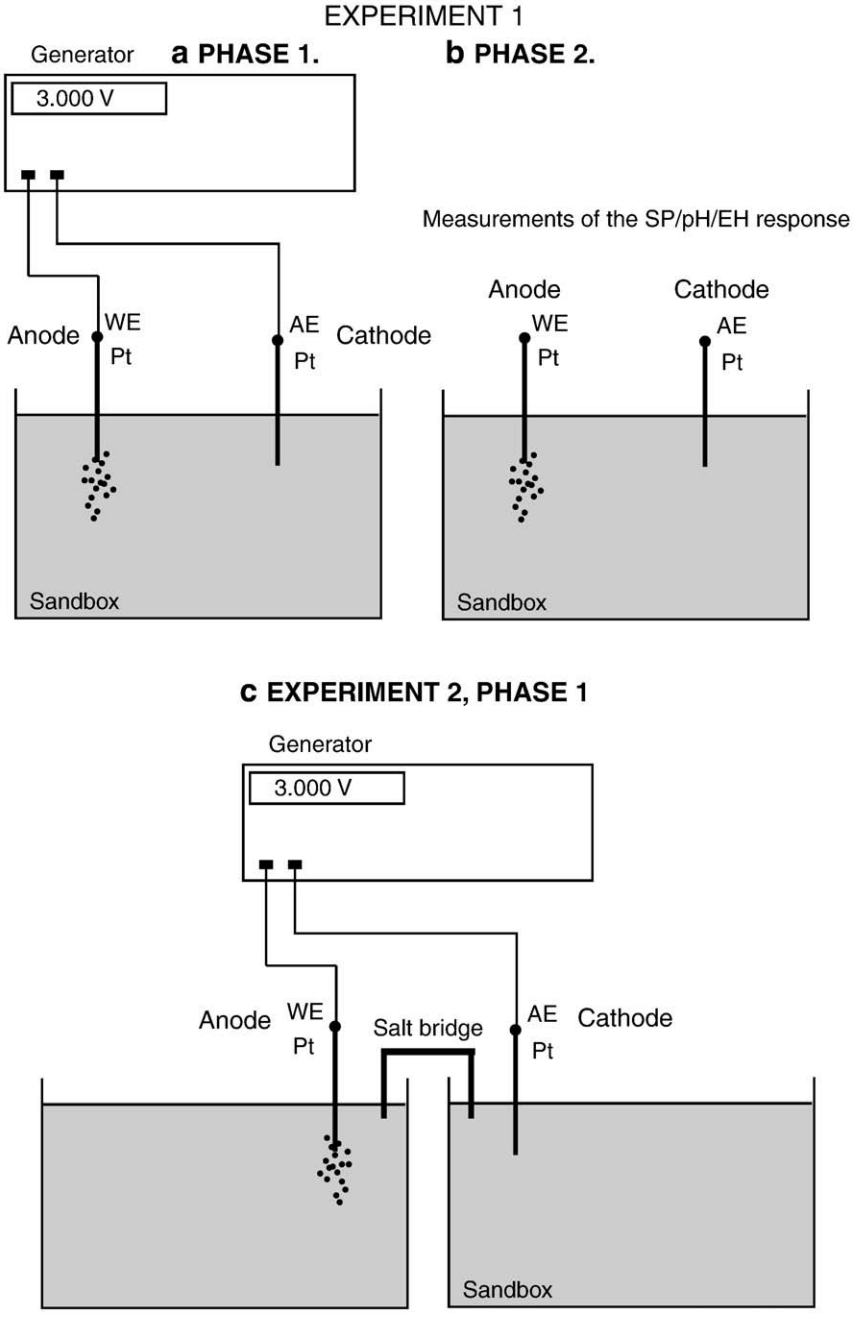

Fig. 1. Sketch of the experimental setups. a. Experiment 1. In Phase 1, a current generator is used to favor electrolysis reaction during 6 days. The amount of electrons released at the anode is the same as those introduced at the cathode. b. In Phase 2, the measurement of self-potential (SP), pH, and redox potential (E_H) is performed at different time intervals. Metallic particles of fougerite are observed to be formed at the working electrode. c. Experiment 2, Phase 1.

Plexiglas™ sandbox (Fig. 1a and b). In the second experiment, they were located in two distinct sandboxes connected together with a saline (agar) bridge (Fig. 1c). Their dimensions were 56 cm in length, 36 cm width, and 17 cm depth. The sand had a lognormal grain size distribution with a grain size comprised between 100 and 160 μm and a mean grain size of 132 μm. The porosity of the sand is 0.34 ± 0.01. X-ray diffraction (XRD) analysis showed that it contained 95% silica, 4% orthoclase feldspar, and less than 1% albite. The sand was saturated by an electrolyte solution composed of ultra pure water (18 MΩ, ultra violet treatment) plus 0.01 mol L^{-1} KCl (Labosi®), 0.0035 mol L^{-1} $FeSO_4$ (Labosi®), and 135 μL L^{-1} of formaldehyde (Sigma®). Formaldehyde was added to the electrolyte to prevent the growth of bacteria. Possible adverse effects of the presence of 135 μL L^{-1} of formaldehyde in the pore water were evaluated, and showed no change in the pH and redox potential of the solution. Additionally, the electrical conductivity and pH of the solution were measured in several places and were determined to be uniform with the conductivity equal to 0.110 S m^{-1} at 25 °C and with the initial pH in the tank equal to 5.5.

To optimize the parameters of the electrolysis, preliminary tests were made to induce redox reactions in well-defined regions of the sandbox. The goal was to create strong redox fronts with known physico-chemical characteristics at known locations. The tension between the two platinum electrodes was tested in the range 1 to 4 V. The amount of electrons produced at the anode is the same as those released at the cathode. Chemical redox reactions were found to occur for a voltage of at least 3 V for a reasonable time frame (5 days). The depth of the Pt electrodes was selected to be at 3 cm after different tests.

The pH was measured with a pH-meter (WTW®, pH 330/SET-1 type) and a combined electrode pH (WTW®, pH/T

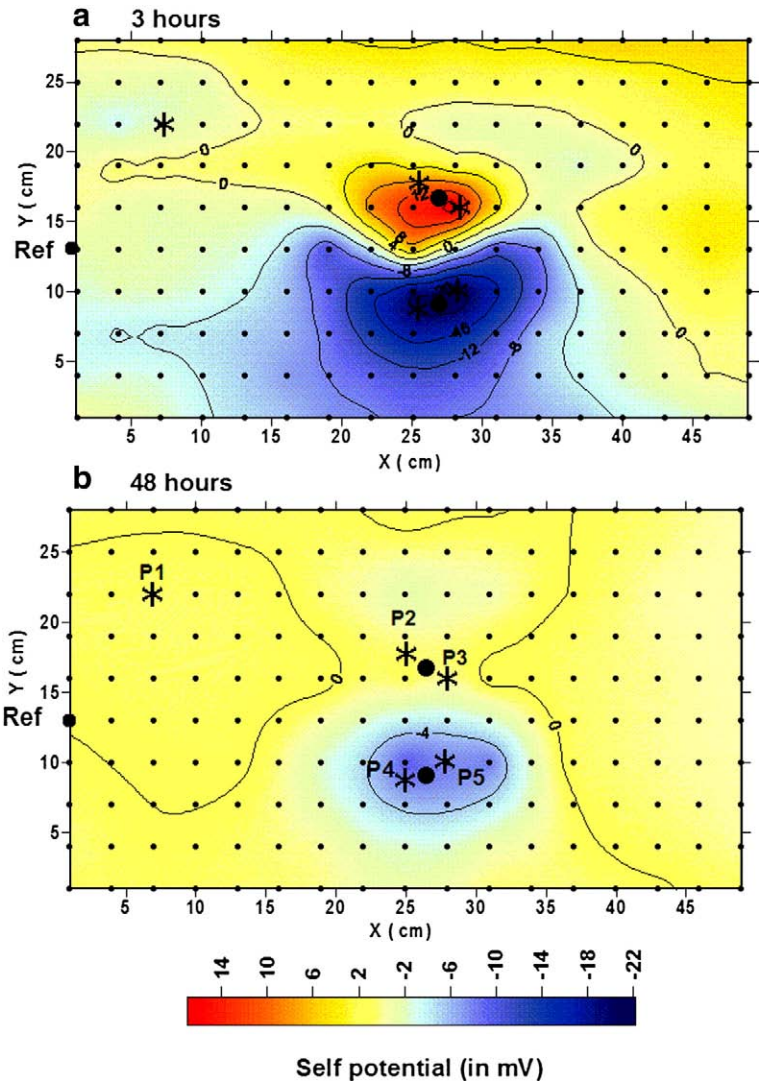

Fig. 2. Distribution of the self-potential at the top surface of the tank for Experiment 1 (Phase 2). The measurements are taken (a) 3 h and (c) 48 h after direct current was turned off. Their location is marked by the small filled circles on the maps. The two filled circles in the middle of the tank represent the position of the working and auxiliary electrodes. The stars (labeled P1 to P5) represent the locations where the self-potential was measured over a depth interval. "Ref" corresponds to the position of the reference electrode.

SENTIX 41 type). The redox potential was measured with redox combination electrodes (InLab501 from Mettler Toledo®); the data ($E_{Ag/AgCl}$) can be converted to the normal hydrogen electrode value (E_{NHE}) using $E_{NHE} = E_{Ag/AgCl} + 208.56$ mV (Macaskill and Bates, 1978). Values of the redox potential were corrected using this formula.

The self-potential signals were measured with a couple of Ag/AgCl non-polarizing electrodes (REF321/XR300 from Radiometer Analytical®) and a calibrated voltmeter (MX-20 from Metrix with a sensitivity of 0.1 mV). One electrode (the reference electrode) was kept fixed at the edge of each sandbox. This electrode was labeled "Ref" on the self-potential maps. The electrode used to scan the electrical potential with respect to the reference electrode (called the roving electrode below) was moved at each self-potential station following a regular lattice pattern at the surface of the tank. All the self-potential data displayed below were corrected from the static difference of electrical potential between the electrodes, which was checked at the beginning and at the end of each set of measurements.

3.1. Experiment 1

In this experiment, the anode and the cathode were placed in the same sandbox (Fig. 1a and b). Once the box was filled with sand saturated with electrolyte solution described above, the system was kept quiet during 12 h for self-compaction of the sand. Then the applied voltage (3 V) was maintained during 6 days (Phase 1). A dark precipitate was observed around and below the working electrode (anode). Thermodynamic calculations and the analysis of XRD data indicate that this precipitate was GR-SO_4 where GR stands for green rust (see Appendix A). The pH, the redox potential, and the self-potential distribution were mapped at different time intervals (30 min, 3 h, and 48 h) after the direct current of the DC power supply was turned off (Phase 2). The distribution of the self-potential data at the top surface of the tank is shown in Fig. 2 and the distribution of the redox potential is shown in Figs. 3 and 4. A decrease of the self-potential anomaly over time was observed. The roving electrode was also used to scan the self-potential signals at a set of depths (2, 4, 6, and 8 cm) at 5 distinct locations labeled P1 to P5 (Fig. 5). The (x, y) coordinates of these points (in cm) were P1(7,22), P4(25,8),

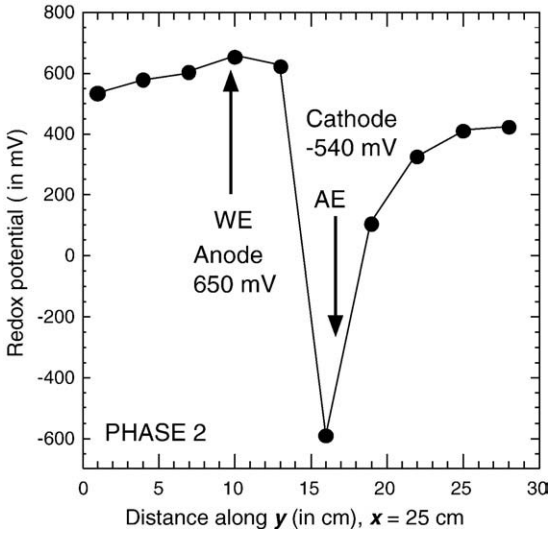

Fig. 4. Distribution of the corrected redox potential across a profile in the tank (along y at $x = 25$ cm, see Fig. 3). The measurements are taken at a depth of 3 cm, 3 h after the DC power supply was shut down at the end of Phase 1. The two arrows show the position of the working (anode) and auxiliary (cathode) electrodes.

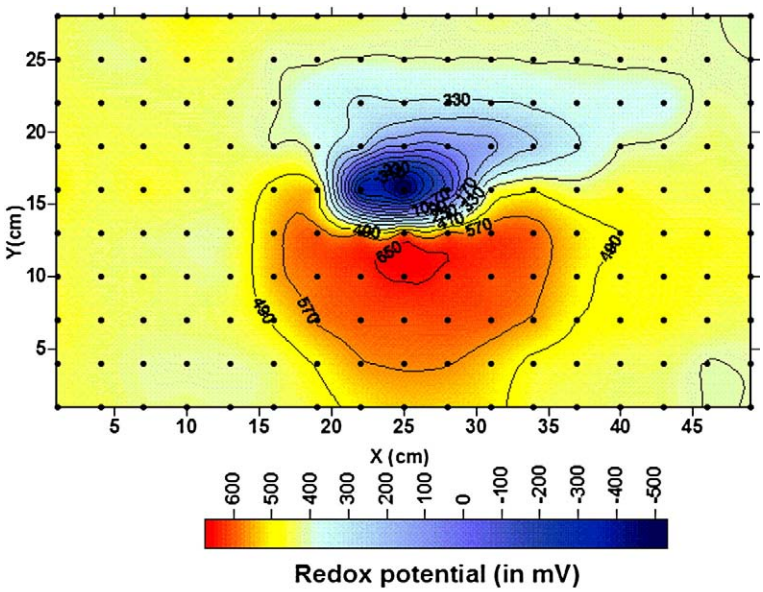

Fig. 3. Distribution of the corrected redox potential inside the tank, at a depth of 3 cm, 3 h after the DC power supply was shut down. The peaks of the dipolar anomaly agree with the position of the anode and the cathode. The shape of this anomaly is quite similar to the self-potential anomaly measured at the top surface of the tank at the same time (see Fig. 2a). Because we used Ag/AgCl electrodes, the correction is $E_{NHE} = E_{Ag/AgCl} + 208.56$ mV where T is the temperature in °C.

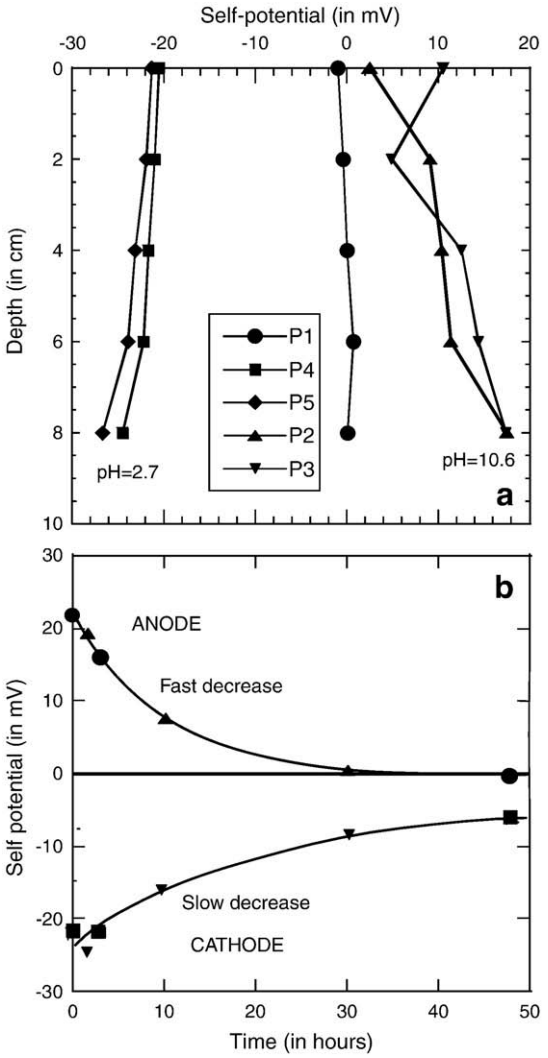

Fig. 5. Variation of the self-potential signals with depth and time with respect to the reference electrode. a. Self-potential signals versus depth 3 h after the DC power supply was shut down. These profiles are shown at 5 distinct locations in the tank (see *x* and *y* coordinates on Fig. 2b and c). b. Self-potential signals versus time at 1 cm from the working and auxiliary electrodes.

P5(28, 10), P2(25,18), and P3(28,16). The self-potential signals do not vary significantly with depth. This experiment was repeated several times and found to be repeatable to within 10%.

3.2. Experiment 2

To avoid having the two self-potential anomalies partly superimposed, the experiment as previously discussed was repeated, but with the cathode and the anode into two identical and separate sandboxes connected by a salt bridge. The salt bridge was built up with a flexible capillary containing a gel obtained by mixing 100 mL of hot water, 30 g KCl, and 3 g of agar-agar and its electrical conductivity was 0.060 S m^{-1} at 25 °C. Additional combined redox electrodes connected to a data logger (Lascar EL2-2-12 bit, Easy-log data logger) were placed at 4 cm from each electrode of electrolysis continuously monitoring and recording the redox potential. As in Experiment 1, the system was kept quiet during 12 h; then the electrolysis reaction was conducted during 6 days with regular stops of the application of direct current each time after 22 h of operation (each stop was 2 h long) permitting the acquisition of the kinetic self-potential distributions at the surface of each box and with pH measurements near the electrolysis electrodes. After 6 days, the pH and both the redox and self-potential distributions were measured 30 min, 3 h, and 48 h after the shut down of the DC power supply. Two horizontal profiles of the pH, the redox potential, and the self-potential are shown in Fig. 6. The results of the experiment for Phase 1 are shown in Figs. 7 and 8. The self-potential anomaly in the vicinity of the cathode grows nearly linearly with time. Its minimum is shown to be ~−7 to −9 mV (Fig. 7). The surface area of the self-potential positive anomaly is several times smaller at the anode by comparison with the cathode. Its maximum is between 7 and 13 mV (Fig. 7). Phase 2 shows similar results as the first experiment and are not shown here.

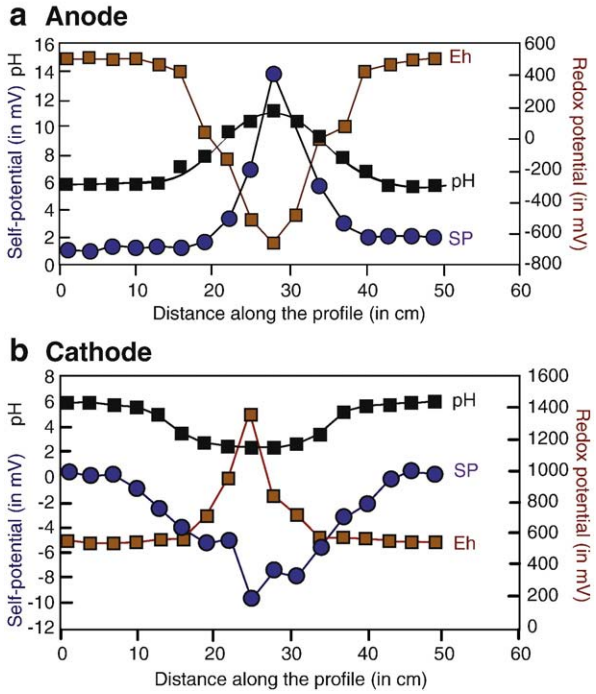

Fig. 6. Distribution of the redox potential, self-potential, and pH along two profiles in Experiment 2. Profile 1 passed through the position of the anode ($y = 16$ cm) and the second profile passed through the position of the cathode in the second tank ($y = 46$ cm).

4. Nature of the self-potential signals

4.1. Description of Phase 1

During Phase 1, a fixed potential was applied during 6 days of operation causing cations and anions to accumulate at the cathode and anode, respectively. Electrolysis of water also causes large changes in the pH, speciation of the aqueous components, and precipitation of Fe-hydroxides (green rust)

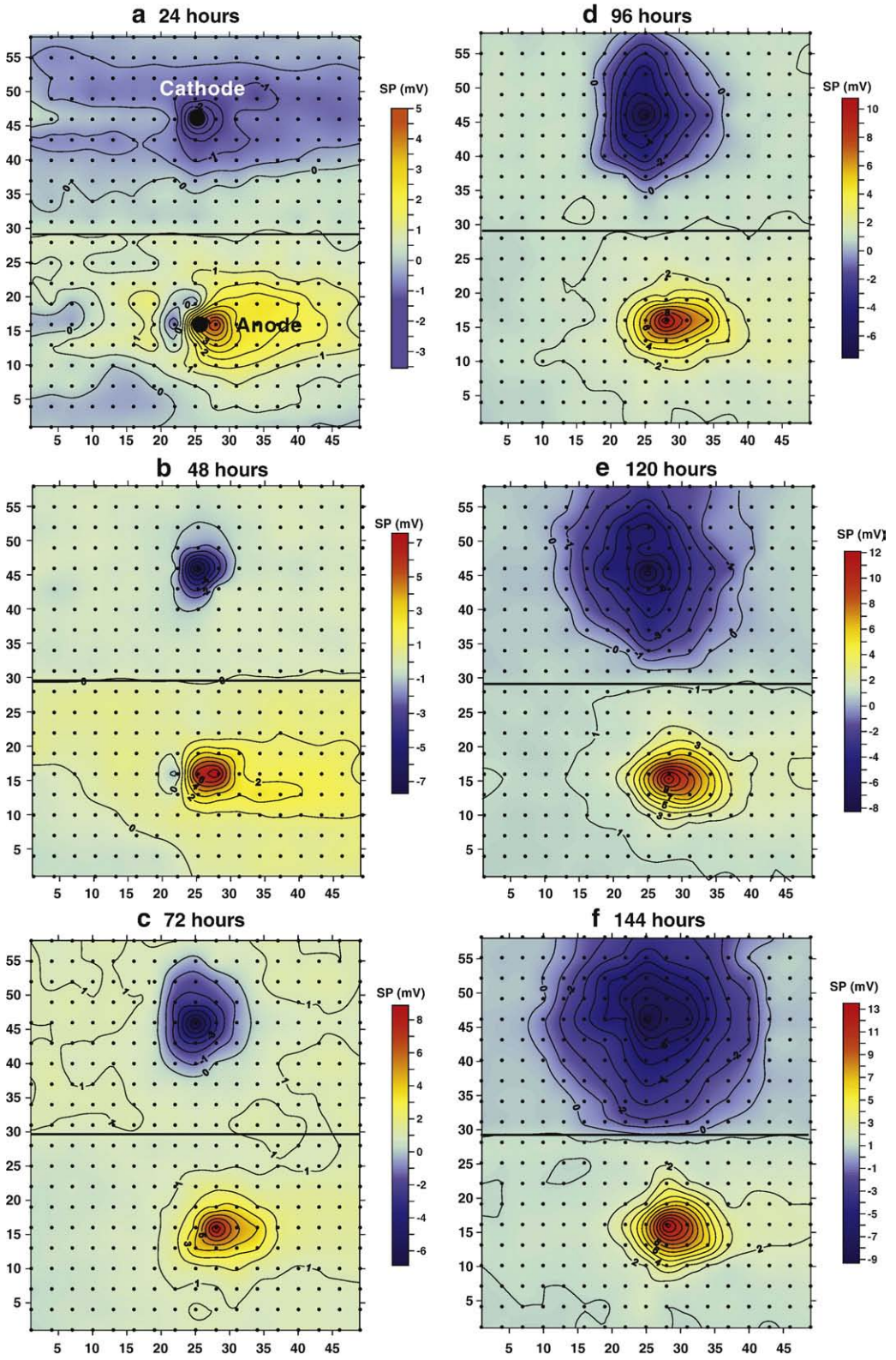

Fig. 7. Map of the self-potential (SP) at different time intervals during Phase 1 (Experiment 2, total duration of Phase 1: 6 days). To measure the self-potential, the DC power supply was shut down for 2 h. The two reservoirs are connected by a salt bridge (see Fig. 1c). The black dots indicate the stations where the self-potential was measured.

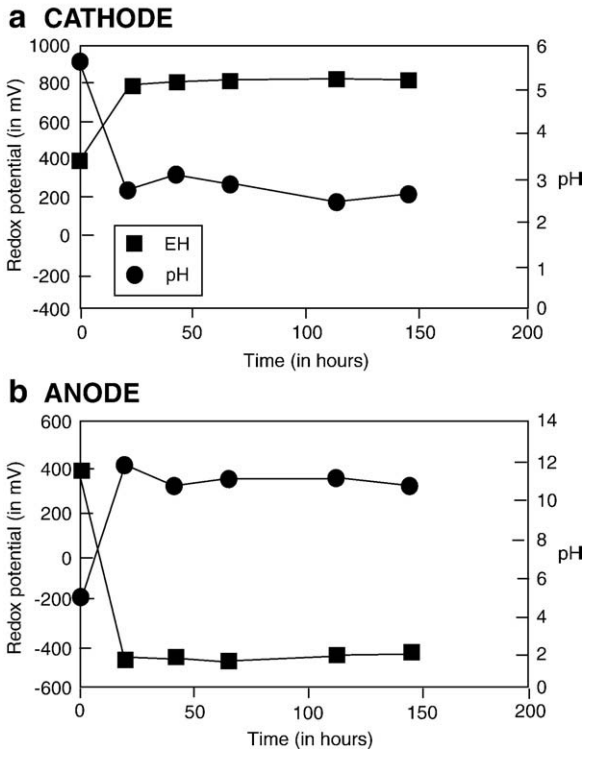

Fig. 8. Evolution of the pH and the redox potential at the cathode and at the anode as a function of time (Experiment 2, Phase 1, total duration of Phase 1: 6 days).

at the anode. The ionic species that were in solution are Fe^{2+}, Cl^-, SO_4^{2-}, K^+, H^+, and OH^-. The cation Fe^{3+} was not present because it is used to form the green rust at the anode. There were three transport processes of transport at work in Phase 1: electromigration, electroosmosis, and diffusion. Their relative efficiency can be compared by comparing their respective characteristic time scales. Figs. 9a and b shows the possible electrochemistry during Phases 1 and 2, respectively.

Electromigration is the transport of ions under the influence of an electrical field. The velocity of an ion is given by the product of its mobility and the magnitude of the electrical field. The characteristic time scale for electromigration is therefore given by,

$$\tau_e = \frac{L}{\beta E} = \frac{L^2}{\beta \delta\psi}, \tag{4}$$

where β is the value of the mobility of a given ion, E the norm of the electrical field, $\delta\psi$ is the applied electrical potential, and L is the distance between the two electrodes. Taking for example $\beta(OH^-) = 20.6\times10^{-8}$ m^2 s^{-1} V^{-1}, $L = 6$ cm (see Experiment 1), and $\delta\psi = 3$ V, we obtain $\tau_e \approx 1.6$ h. This is a very short term by comparison with the total duration of Phase 1 (6 days) so it was concluded that electromigration was a very effective transport mechanism during Phase 1. This mechanism drives the accumulation of H^+ at the cathode (resulting in a low pH at the cathode). It drives also the accumulation of OH^- at the anode explaining the high pH at the anode. The source of H^+ and OH^- is provided directly by the decomposition of the water molecules and this source is therefore present everywhere in the sandbox.

In general, an electrical field applied to a water-saturated porous material is responsible for the flow of the pore water. This flow is explained, at the microscopic level, by the viscous drag of the pore water by the excess of electrical charge existing into the diffuse layer coating the surface of the grains, and is called electroosmosis. This occurs in the direction of the electrical field for pH greater than the point of zero charge (pzc) of the mineral surface (typically pH(pzc) = 3 for silica). The flow is in the opposite direction of the electrical field for pH below pH(pzc). Using the model developed by Revil and Leroy (2004) and Revil et al. (2005), the characteristic time scale of electroosmosis is given by,

$$\tau_h = \frac{L^2 \eta_f \phi}{k \overline{Q}_V \delta\psi}, \tag{5}$$

where the value of the porosity is given by $\phi = 0.34$, $\eta_f = 10^{-3}$ Pa s, the value of the permeability is $k = 7.3\times10^{-12}$ m^2 (determined by a constant head method), and the excess of charge (of the diffuse layer) per unit pore volume is $\overline{Q}_V = 0.77$ C m^{-3} (see Crespy et al., 2008 who used the same sand than in our experiment). This yields a characteristic time constant equal to 20.6 h. This value is smaller than the duration of Phase 1, so electroosmosis is an effective transport mechanism during Phase 1, but it is much less effective than electromigration. Because the pH in the vicinity of the cathode is close to 3, this process in not effective in the vicinity of the cathode.

A third mechanism of transport is diffusion of the ions resulting from the existence of a gradient in their chemical potential. The characteristic time scale for diffusion is,

$$\tau_d = \frac{L^2}{D}, \tag{6}$$

where D is the diffusion coefficient (in m^2 s^{-1}). Taking $L = 6$ cm and $D = 2\times10^{-9}$ m^2 s^{-1}, a characteristic time constant of 21 days is calculated. This is a very long characteristic time by comparison with the two previous processes, and was determined to be the least significant process.

Consequently, electromigration was the main transport mechanism in Phase 1 and explains why the value of the pH and the redox potential reaches steady-state values very quickly (Fig. 8) at the anode and the cathode. The analysis of the pH at the anode and at the cathode (2.8 at the cathode and 10.8−11.2 at the anode) indicates that approximately $10^{-2.8}$ mol L^{-1} of H^+ and OH^- were generated in Phase 1 of the second experiment.

4.2. Description of Phase 2

At the end of Phase 1, the DC power supply was shut down and all of the species that had accumulated at the anode and cathode (Fe^{2+}, Cl^-, SO_4^{2-}, K^+, H^+, and OH^-) diffuse freely in their concentration fields. Additionally, the oxidation of the fougerite at the anode yielded goethite and released sulfate. In Phase 2, noticeable self-potential anomalies can be associated with the redox front observed in Fig. 3. The redox potential gradient resulting from electromigration

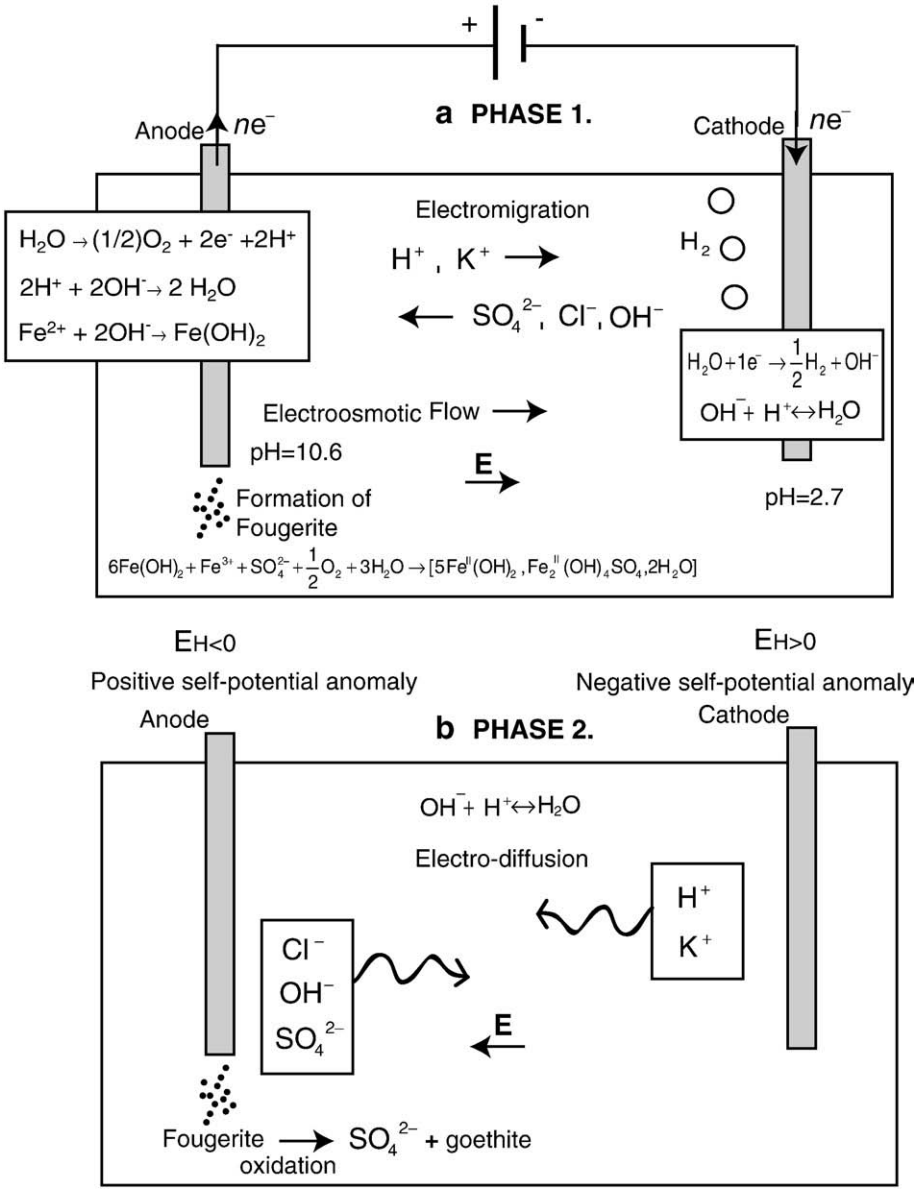

Fig. 9. Transfer of charge and electrochemical reactions in the two phases of the experiment. Note that in Phase 2, there is a source term for the diffusion of sulfate and iron III at the anode corresponding to the oxidation of the fougerite formed in Phase 1.

during Phase 1 was over 20 V/m. This is a very strong value. However, the observed self-potential anomalies amounted only to few tens of millivolts. These anomalies are therefore much smaller than the anomalies expected in the presence of an electronic conductor bridging a sharp redox front (see Sato and Mooney, 1960, for ore bodies, Castermant et al., 2008 for the corrosion of an iron bar in a sandbox, Arora et al., 2007, for contaminant plumes, and Ntarlagiannis et al., 2007, for a biotic column experiment). In the presence of an electronic conductor, the expected self-potential anomalies can amount several hundreds of millivolts. The diagram of stability of fougerite is shown in Fig. 10. It is built using the reactions displayed in Table 1.

The self-potential tomographic algorithm developed by Jardani et al. (2007, 2008) was used to determine the position of the source current density $\mathbf{j}_S$ responsible for the self-potential signals. As expected, the tomography revealed two sources of the self-potential signals corresponding to two elongated source volumes located at the position of the platinum electrodes with maxima just below the electrodes (Fig. 11). The fact that the maxima of the source current densities were located below the two electrodes was not surprising, because the concentrations of the identified species in the pore water increased over time in the vicinity of the electrodes. This created a pore solution that was denser than the surrounding pore fluid. The fact that the source of the observed self-potential anomalies were shown to be elongated vertical source volumes also explains the approximate depth invariance of the electrical potentials (see Fig. 5a). At the anode, the precipitation of fougerite that

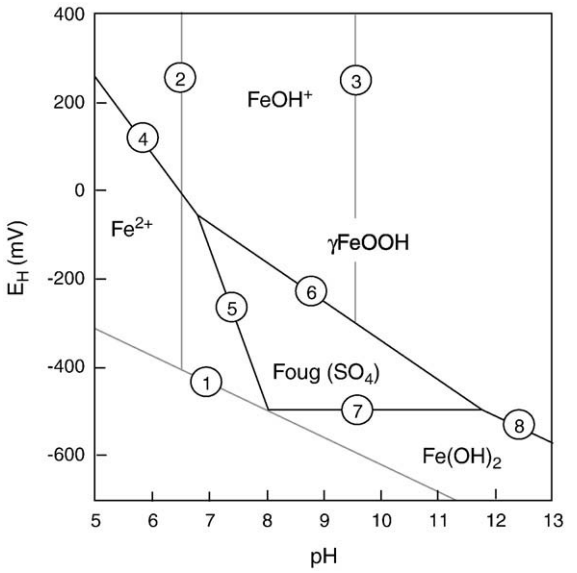

Fig. 10. Stability diagram for SO_4-GR (fougerite). The initial activities of the species in the experimental conditions: $\log[Fe^{2+}] = -2.76$, $\log[FeOH^{+}] = -5.260$, and $\log[SO_4^{2-}] = -2.783$.

occurred in Phase 1 was observed mostly a little below the anode (see Section 3).

5. Discussion

The previous analysis implies that the potential contribution of the ions in generating self-potential anomalies is relatively small with only few tens of millivolts of self-potential anomalies. Clearly, this cannot explain the giant (>300 mV) self-potential anomaly observed above contaminant plumes like the one associated with the landfill of Entressen, in the south of France (Naudet et al., 2003). Naudet et al. (2003) also observed a very strong correlation between the self-potential signals (corrected for the streaming potential contribution associated with the flow of the ground water) and the in situ measurements of the redox potential in the contaminated aquifer. We can explain this observation as follows.

The Hittorf number t_i of species i (dimensionless) represents the fraction of electrical current carried by species . It is defined by,

$$t_i = \frac{\beta_i C_i |q_i|}{\sum_{i=1}^{N+1} \beta_i C_i |q_i|}, \tag{7}$$

for $i = 1,...N+1$ (N-ionic species, the notation "+1" corresponds to electrons as an additional species) and where β_i the mobility of species i. If an electronic conductor is present in the system, the mobility of electrons in this electronic conductor is much higher than the mobility of the ions in the pore space of the porous material (Bockris and Reddy, 1970). This means that the Hittorf numbers for the dissolved species 1, N are zero and that for the electron is ~1. Using Eq. (3) with $q_{e^-} = -e$ where e is the elementary charge, the source current density can be written as,

$$\mathbf{j}_S = \frac{k_b T}{e} \sigma \nabla ln\{e^-\}, \tag{8}$$

where $\{e^-\}$ represents the effective activity of the electrons. The relative electron activity, as an intensity parameter for the pore water, is defined as $p\varepsilon = -\log\{e^-\}$ (e.g., Christensen et al., 2000). The redox potential (in V) is defined through the Nernst equation by (e.g., Christensen et al., 2000),

$$E_H = 2.3 \frac{k_b T}{e} p\varepsilon, \tag{9}$$

where T is the absolute temperature in K, and k_b is the Boltzmann constant. With these definitions, we obtain,

$$\mathbf{j}_S = -\sigma \nabla E_H, \tag{10}$$

which provides a theoretical foundation to the works made by Linde and Revil (2007) who used Eq. (10) to establish a relationship between the self-potential and redox potential over the contaminant plume of Entressen (see Arora et al., 2007). Linde and Revil (2007) used Eq. (10) to invert the self-potential signals recorded at the ground surface downstream

Table 1
Redox reaction for the stability domain of SO_4-fougerite.

Chemical reactions		Equilibrium relationships
$H_2 \leftrightarrows 2H^+ + 2e^-$ [a]	(1)	$E_H = 0.000 - 0.0591$ pH
$Fe^{2+} + H_2O \leftrightarrows FeOH^+ + H^+$ [b]	(2)	$8.98 = \log[Fe^{2+}] - \log[FeOH^+] + pH$
$FeOH^+ + H_2O \leftrightarrows Fe(OH)_2 + H^+$ [b]	(3)	$4.35 = \log[FeOH^+] + pH$
$Fe^{2+} + 2H_2O \leftrightarrows \gamma FeOOH + 3H^+ + e^-$ [b]	(4)	$E_H = 0.99 - 0.0591 \log[Fe^{2+}] - 0.1773$ pH
$Fe(OH)_2 \leftrightarrows \gamma FeOOH + H^+ + e^-$ [b]	(5)	$E_H = 0.197 - 0.0591$ pH
$6Fe^{2+} + SO_4^{2-} + 12H_2O + \leftrightarrows + Fe_6(OH)_{12}SO_4 + 12H^+ + 2e^-$ [c]	(6)	$E_H = 1.78 - 0.1773 \log[Fe^{2+}] - 0.0296 \log[SO_4^{2-}] - 0.3546$ pH
$Fe_6(OH)_{12}SO_4 \leftrightarrows 6\gamma FeOOH + SO_4^{2-} + 6H^+ + 4e^-$ [c]	(7)	$E_H = 0.59 + 0.0148 \log[SO_4^{2-}] - 0.0887$ pH
$6Fe(OH)_2 + SO_4^{2-} \leftrightarrows Fe_6(OH)_{12}SO_4 + 2e^-$ [c]	(8)	$E_H = -0.57 - 0.0296 \log[SO_4^{2-}]$

[a] Water stability domain.
[b] Iron species.
[c] Sulfate containing media.

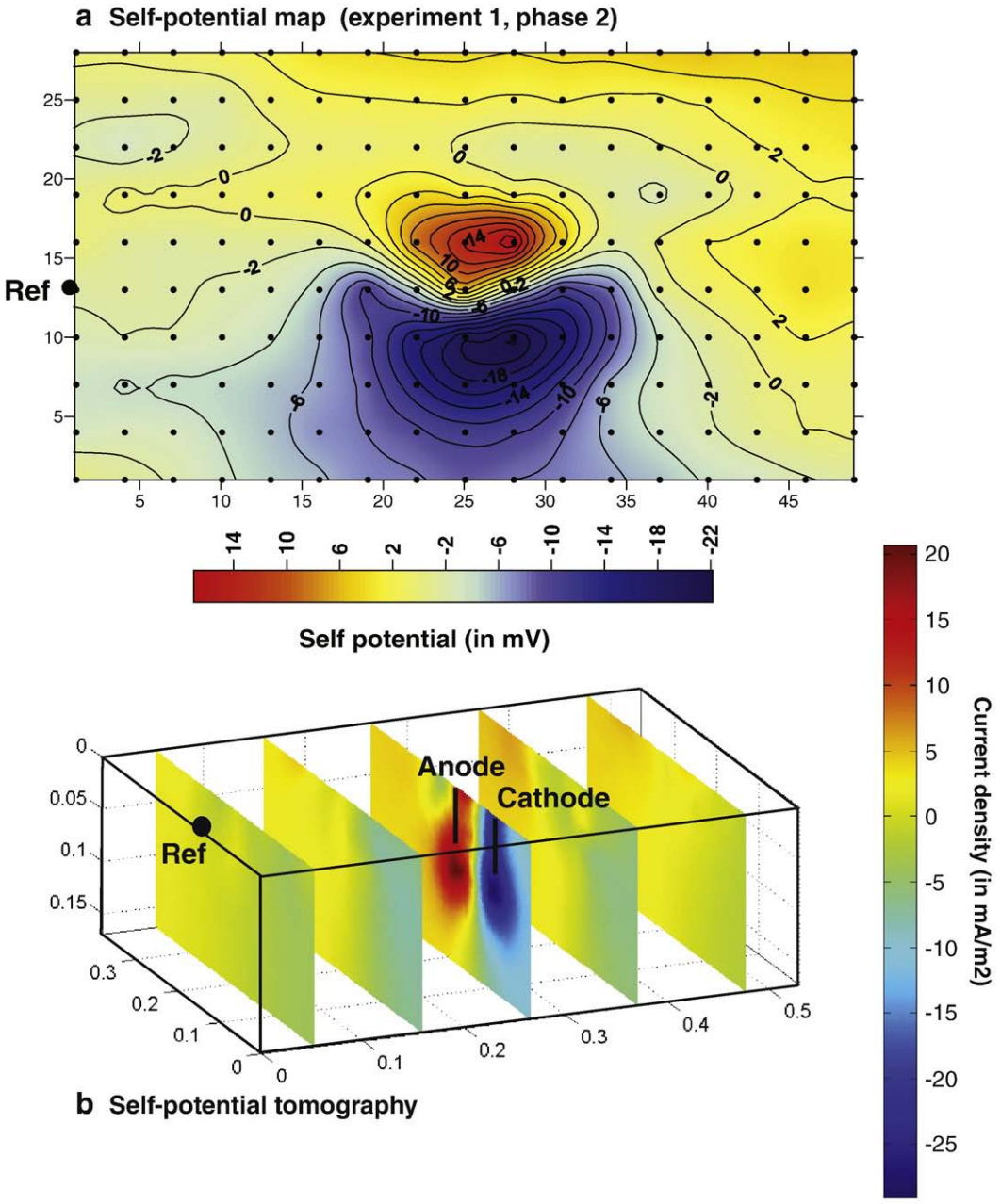

Fig. 11. Tomography of the self-potential signals 3 h after the DC power supply was shut down. The tomography shows that the positions of the two sources of electrical current are vertical sources with the maximum in the source current density located below both the cathode and the anode.

the landfill of Entressen in the South of France in the purpose of determining the distribution of the redox potential in the contaminated unconfined aquifer. They also used electrical resistivity tomography for the distribution of the electrical conductivity of the ground. They were successful in retrieving the in situ distribution of the redox potential in the unconfined aquifer of Entressen assuming that the source current density was located in the capillary fringe where a sharp transition in the redox potential is often noticed (Wadey et al., 2001; Ashworth and Shaw, 2006). This implies that a possibly biotic electronic conductor should be present at the capillary fringe of the unconfined contaminated aquifer.

Because there are no free electrons in the pore water, if an electronic conductor is required to bridge electron donors and electron acceptors in the capillary fringe, one may wonder about the nature of this electronic conductor. While the answer to this question deserves a paper in itself, a brief explanation for a potential mechanism can be envisioned in a contaminant plume that is rich in organic matter and a porous material characterized by a small capillary fringe. Reguera et al. (2005), Gorby et al. (2006), and Ntarlagiannis et al.

(2007) showed that both *Geobacter sulfurreducens* and *Shewanella oneidensi* have, under specific conditions, conductive pili that can serve as electronic conductors between electron donors and electrons acceptors. While geobacter works only in anerobic conditions, *S. oneidensi* is a facultative adaptive bacteria that can use oxygen as terminal electron acceptor. The pili of *G. sulfurreducens* have an electrical conductivity in the range 100 to 1000 S m^{-1} (Reguera et al., 2005). Bacterial cells of *S. oneidensi* containing deletion mutations in the pilD gene and that do not produce conductive pili do not produce strong self-potential signals (Gorby et al., 2006; Ntarlagiannis et al., 2007). Networks of pili have also been observed by E. Atekwana at the fringe of a contaminant plume (E. Atekwana, personal communication, 2008).

Because bacteria are very effective catalysts, they also lower the activation energy between electron donors and electron acceptors. All these observations suggest that bacteria may have a strong role in the type of geobattery existing in contaminant plumes. This potential role of bacteria needs however to be further investigated before definitive conclusions can be reached but this finding has very strong potential applications including for bioremediation of contaminant plumes because the process can be inverted (providing electrical energy to increase the metabolism of the bacterial communities).

6. Conclusion

There are two main conclusions that can be drawn from the experiments discussed in the work described here. The former is related to the fact that only modest self-potential signals are generated in a porous material in the absence of an electronic conductor but in the presence of a sharp redox potential gradient. While the model described by Arora et al. (2007), Linde and Revil (2007), and Castermant et al. (2008) predicts self-potential signals of the same order of magnitude as the redox potential in the presence of an electronic conductor (in agreement with field and laboratory observations), the experiments described above show that only a few tens of millivolts are produced through a 20 V/m sharp redox potential front. This implies in turn that an electronic conductor should be present in the field to explain the very strong self-potential anomalies observed by Arora et al. (2007) and Linde and Revil (2007).

The second conclusion is that despite their small magnitudes, the diffusion potentials observed in our experiments were measurable and can be easily observed in the field in cases where there is no contribution from the transfer of electrons through a biotic or an abiotic electronic conductor. New devices have been developed recently from electroencephalography and applied to geophysical self-potential problems (Crespy et al., 2008). They allow to measure self-potential signals with a very high accuracy (submicrovolts).

The coupling of the modeling of self-potential signals (Maineult et al., 2005, 2006; Linde and Revil, 2007) and DC-resistivity signals (Shevnin et al., 2005) to reactive/transport codes (including the important role of biochemistry, see Hunter et al., 1998) is a very important step to predict the value of the self-potential signals and resistivity data over contaminant plumes. In turn, this implies that the inversion of these (geophysical) signals would be possible, inside a stochastic framework, to constrain the electro(bio)chemistry at play in certain types of contaminant plumes, like those associated with landfills.

Acknowledgments

We thank the Institut National de Recherche Agronomique (INRA), the CNRS, and the Region Provence-Alpes-Côtes-d'Azur (PACA) for their support in France. This research is also supported by the Office of Science (BER), U.S. Department of Energy, Grant No. DE-FG02-08ER64659. The grant of Julien Castermant is supported by Région PACA and INRA in France.

Appendix A

X-ray measurements (XRD) were performed with a sample of sand collected in the tank at a position where the sand colored in a blue–green color just below the position of the anode. Once taken, this sample was immediately placed in the X-ray diffraction apparatus (PANalytical, Co-Kalpha1, theta/theta) before it gets oxidized by air. The characteristic peaks observed for the sand used in this study were observed plus an additional small peak at 11.0–11.6 Å. This peak is consistent with the main 001 peak of the GR-SO_4 where GR stands for green rust (Trolard and Bourrié, 2008). This peak cannot be misled with the peak associated with mixed-layer clays because no such clays were present in the sand.

We show now that the SO_4-green rust is stable accounting for the conditions of pH, E_H, and Fe. Because of the presence of both chloride and sulfate, two possible forms of fougerite are GR-Cl (corresponding to $Fe_3(II)Fe_1(III)(OH)_8\cdot Cl$) and GR-$SO_4$ (corresponding to $Fe_4(II)Fe_2(III)(OH)_{12}\cdot SO_4$). The two reactions for the formation of these two green rusts are,

$$Fe_4(II)Fe_2(III)(OH)_{12}\cdot SO_4 + 12H^+ + 2e^- \Leftrightarrow 6Fe^{2+} + SO_4^{2-} + 12H_2O, \quad (A1)$$

$$Fe_3(II)Fe(III)(OH)_8\cdot Cl + 8H^+ + e^- \Leftrightarrow 4Fe^{2+} + Cl^- + 8H_2O. \quad (A2)$$

There is a competition between the two reactions, which can be combined to give,

$$2GR-SO_4 + 3Cl^- + e^- \Leftrightarrow 3GR-Cl + 2SO_4^{2-}, \quad (A3)$$

$$\log Q = 2\log[SO_4^{2-}] - 3\log[Cl^-] - \log[e^-]. \quad (A4)$$

In the pore water solution, the concentration in KCl is 0.01 M and the concentration in $FeSO_4$ is 0.0035. The corrected redox potential is −469 mV. This yields a $p\varepsilon = -7.95$. We used PHREEQC (Parkhurst and Appelo, 1999) to compute the speciation in the pore water solution. This yields $\log Q = -7.32$. We can compute now the equilibrium constant of reaction (A3). Using the Gibbs free energy of formation of the various components implied in reaction (A3), we obtain $\log K = -8.69$. Because $\log Q > \log K$, we can conclude that the sulfate form of the green rust is stable. The ideal setting for the precipitation of SO_4-green rust is a pH comprised between 8 and 11 and a redox potential comprised between −540 mV and −469 mV. This represents a non-negligible volume in the tank in the vicinity of the anode.

References

Arora, T., Revil, A., Linde, N., Castermant, J., 2007. Non-intrusive determination of the redox potential of contaminant plumes using the self-potential method. Journal of Contaminant Hydrology 92 (3–4), 274–292.

Ashworth, D.J., Shaw, G., 2006. A comparison of the soil migration and plan uptake of radioactive chlorine and iodine from contaminated groundwater. Journal of Environmental Radioactivity 89, 1–80.

Bigalke, J., Grabner, E.W., 1997. The geobattery model: a contribution to large scale electrochemistry. Electrochimica Acta 42, 3443–3452.

Bockris, J.O.'M., Reddy, A.K.N., 1970. Modern Electrochemistry, vol. 2. Plenum Press, New York. 1432 pp.

Bolève, A., Crespy, A., Revil, A., Janod, F., Mattiuzzo, J.L., 2007. Streaming potentials of granular media: influence of the Dukhin and Reynolds numbers. Journal of Geophysical Research 112, B08204. doi:10.1029/2006JB004673.

Castermant, J., Mendonça, C.A., Revil, A., Trolard, F., Bourrié, G., Linde, N., 2008. Redox potential distribution inferred from self-potential measurements during the corrosion of a burden metallic body. Geophysical Prospecting 56, 269–282. doi:10.1111/j.1365-2478.2007.00675.x.

Christensen, T.H., Bjerg, P.L., Banwart, S.A., Jakobsen, R., Heron, G., Albrechtsen, H.-J., 2000. Characterization of redox conditions in groundwater contaminant plumes. Journal of Contaminant Hydrology 45, 165–241.

Corwin, R.F., Hoover, D.B., 1979. Self-potential method in geothermal exploration. Geophysics 44 (2), 226–245.

Crespy, A., Bolève, A., Revil, A., 2007. Influence of the Dukhin and Reynolds numbers on the apparent zeta potential of granular media. Journal of Colloid and Interface Science 305, 188–194.

Crespy, A., Revil, A., Linde, N., Byrdina, S., Jardani, A., Bolève, A., Henry, P., 2008. Detection and localization of hydromechanical disturbances in a sandbox using the self-potential method. Journal of Geophysical Research 113, B01205. doi:10.1029/2007JB005042.

Cussler, E.L., 2008. Diffusion. Mass Transfer in Fluid Systems. Cambridge University Press, Cambridge. 631 pp.

Doll, H.G., 1949. The S.P. log: theoretical analysis and principles of interpretation. Transactions of American Institute of Mining, Metallurgical, and Petroleum Engineers 179, 146–185.

Fox, R.W., 1830. On the electromagnetic properties of metalliferous veins in the mines of Cornwall. Philosophical Transactions of the Royal Society 120, 399–414.

Gorby, Y.A., Yanina, S., McLean, J.S., Rosso, K.M., Moyles, D., Dohnalkova, A., et al., 2006. Electrically conductive bacterial nanowires produced by *Shewanella oneidensis* strain MR-1 and other microorganisms. Proceedings of the National Academy of Sciences of the United States of America 103, 11358–11363.

Hunter, K.S., Wang, Y., Van Cappellen a, P., 1998. Kinetic modeling of microbially-driven redox chemistry of subsurface environments: coupling transport, microbial metabolism and geochemistry. Journal of Hydrology 209, 53–80.

Jardani, A., Revil, A., Bolève, A., Dupont, J.P., Barrash, W., Malama, B., 2007. Tomography of groundwater flow from self-potential (SP) data. Geophysical Research Letters 34, L24403. doi:10.1029/2007GL031907.

Jardani, A., Revil, A., Bolève, A., Dupont, J.P., 2008. 3D inversion of self-potential data used to constrain the pattern of ground water flow in geothermal fields. Journal of Geophysical Research 113, B09204. doi:10.1029/2007JB005302.

Linde, N., Revil, A., 2007. Inverting residual self-potential data for redox potentials of contaminant plumes. Geophysical Research Letters 34, L14302. doi:10.1029/2007GL030084.

Macaskill, J.B., Bates, R.G., 1978. Standard potential of the silver–silver chloride electrode. Pure and Applied Chemistry 50, 1701–1706.

Maineult, A., Bernabé, Y., Ackerer, P., 2004. Electrical response of flow, diffusion and advection in a laboratory sandbox. Vadose Zone 3, 1180–1192.

Maineult, A., Bernabé, Y., Ackerer, P., 2005. Detection of advected concentration and pH fronts from spontaneous potential measurements. Journal of Geophysical Research 110 (B11), B11205. doi:10.1029/2005JB003824.

Maineult, A., Bernabé, Y., Ackerer, P., 2006. Detection of advected, reacting redox fronts from self-potential measurements. Journal of Contaminant Hydrology 86, 32–52.

Mendonça, C.A., 2008. Forward and inverse self-potential modeling in mineral exploration. Geophysics 73 (1), F33–F43.

Naudet, V., Revil, A., 2005. A sandbox experiment to investigate bacteria-mediated redox processes on self-potential signals. Geophysical Research Letters 32, L11405. doi:10.1029/2005GL022735.

Naudet, V., Revil, A., Bottero, J.Y., Begassat, P., 2003. Relationship between self-potential (SP) signals and redox conditions in contaminated groundwater. Geophysical Research Letters 30 (21), 2091. doi:10.1029/2003GL018096.

Naudet, V., Revil, A., Rizzo, E., Bottero, J.Y., Begassat, P., 2004. Groundwater redox conditions and conductivity in a contaminant plume from geoelectrical investigations. Hydrology and Earth System Sciences 8 (1), 8–22.

Ntarlagiannis, D., Atekwana, E.A., Hill, E.A., Gorby, Y., 2007. Microbial nanowires: is the subsurface « hardwired »? Geophysical Research Letters 34, L17305. doi:10.1029/2007GL030426.

Parkhurst, D.L., Appelo, C.A.J. 1999. User's guide to PHREEQC (Version 2). A computer program for speciation, batch-reaction, one-dimensional transport, and inverse geochemical calculations. Water-Ressources Investigation Report 99-4259, U.S. Department of the Interior, U.S. Geological Survey, Denver, Colorado.

Peiffer, S., Klemm, O., Pecher, K., Hollerung, R., 1992. Redox measurements in aqueous solutions — a theoretical approach to data interpretation, based on electrode kinetics. Journal of Contaminant Hydrology 10, 1–18.

Personna, Y.R., Ntarlagiannis, D., Slater, L., Yee, N., O'Brien, M., Hubbard, S., 2008. Spectral induced polarization and electrodic potential monitoring of microbially mediated iron sulfide transformations. Journal of Geophysical Research, 113, G02020.

Reguera, G., McCarthy, K.D., Metha, T., Nicol, J.S., Tuominen, M.T., Lovley, D.R., 2005. Extracellular electron transfer via microbial nanowires. Nature 435, 1098–1101.

Revil, A., 1999. Ionic diffusivity, electrical conductivity, membrane and thermoelectric potentials in colloids and granular porous media: a unified model. Journal of Colloid and Interface Science, 212, 503–522.

Revil, A., Leroy, P., 2004. Governing equations for ionic transport in porous shales. Journal of Geophysical Research 109, B03208. doi:10.1029/2003JB002755.

Revil, A., Linde, N., 2006. Chemico-electromechanical coupling in microporous media. Journal of Colloid and Interface Science 302, 682–694.

Revil, A., Leroy, P., Titov, K., 2005. Characterization of transport properties of argillaceous sediments. Application to the Callovo-Oxfordian Argillite. Journal of Geophysical Research 110, B06202. doi:10.1029/2004JB003442.

Sato, M., Mooney, H.M., 1960. The electrochemical mechanism of sulfide self-potentials. Geophysics 25, 226–249.

Shevnin, V., Delgado-Rodriguez, O., Fernandez-Linares, L., Zegarra Martinez, H., Mousatov, A., Ryjov, A., 2005. Geoelectrical characterization of an oil-contaminated site in Tabasco, Mexico. Geofisica International 44 (3), 251–263.

Sivenas, P., Beales, F.W., 1982. Natural geobatteries associated with sulphide ore deposits. I. Theoretical studies. Journal of Geochemical Exploration 17, 123–143.

Stoll, J., Bigalke, J., Grabner, E.W., 1995. Electrochemical modeling of self-potential anomalies. Surveys in Geophysics 16 (1), 107–120.

Trolard, F., Bourrié, G., 2008. Chapter 5. Geochemistry of green rusts and fougerite: a reevaluation of Fe cycle in soils. Advances in Agronomy, 99, 227–288.

Tuccillo, M.E., Cozzarelli, I.M., Herman, J.S., 1999. Iron reduction in the sediments of a hydrocarbon-contaminated aquifer. Applied Geochemistry 14, 655–667.

Wadey, P., Shaw, G., Bell, J.N.B., 2001. Vadose zone processes and chemical transport. Journal of Environmental Quality 30, 1341–1353.